Weierstraß-Institut
für Angewandte Analysis und Stochastik

Leibniz-Institut im Forschungsverbund Berlin e. V.

Preprint ISSN 2198-5855

Modeling and simulation of an isolated mini-grid including battery operation strategies under uncertainty using chance constraints

René Henrion[1], Dietmar Hömberg[1,2,3], Nina Kliche[1]

submitted: September 2, 2024

[1] Weierstrass Institute
Mohrenstr. 39
10117 Berlin
Germany
E-Mail: rene.henrion@wias-berlin.de
dietmar.hoemberg@wias-berlin.de
nina.kliche@wias-berlin.de

[2] Technische Universität Berlin
Institut für Mathematik
Str. des 17. Juni 136
10623 Berlin
Germany

[3] Norwegian University of Science and Technology
Department of Mathematical Sciences
Alfred Getz' vei 1
7034 Trondheim
Norway

No. 3125
Berlin 2024

2020 *Mathematics Subject Classification.* 65K10, 90C15, 90C30.

Key words and phrases. Mini-grid operation, uncertainty management, risk management, probabilistic optimal control.

This work was funded by the German Research Foundation (DFG) under the German National Excellence Strategy – The Berlin Mathematics Research Center MATH+ (EXC-2046) in Project AA4-10.

Edited by
Weierstraß-Institut für Angewandte Analysis und Stochastik (WIAS)
Leibniz-Institut im Forschungsverbund Berlin e. V.
Mohrenstraße 39
10117 Berlin
Germany

Fax: +49 30 20372-303
E-Mail: preprint@wias-berlin.de
World Wide Web: http://www.wias-berlin.de/

Modeling and simulation of an isolated mini-grid including battery operation strategies under uncertainty using chance constraints

René Henrion, Dietmar Hömberg, Nina Kliche

Abstract

This paper addresses the challenge of handling uncertainties in mini-grid operation, crucial for achieving universal access to reliable and sustainable energy, especially in regions lacking access to a national grid. Mini-grids, consisting of small-scale power generation systems and distribution infrastructure, offer a cost-effective solution. However, the intermittency and uncertainty of renewable energy sources poses challenges, mitigated by employing batteries for energy storage. Optimizing the lifespan of the battery energy storage system is critical, requiring a balance between degradation and operational expenses, with battery operation strategies playing a key role in achieving this balance. Accounting for uncertainties in renewable energy sources, demand, and ambient temperature is essential for reliable energy management strategies. By formulating a probabilistic optimal control problem for minimizing the daily operational costs of standalone mini-grids under uncertainty, and exploiting the concept of joint chance constraints, we address the uncertainties inherent in battery dynamics and the associated operational constraints.

1 Introduction

As outlined by the United Nations, 675 million people still lack access to electricity with four out of five residing in sub-Saharan Africa. As an immediate consequence, one sustainable development goal aims at ensuring universal access to affordable, reliable, sustainable and modern energy. This goal encapsulates two primary tasks. The first task is to prioritize universal access to electricity, ensuring that every individual has the fundamental right to reliable power. The secondary task entails decarbonizing the energy sector, transitioning towards cleaner and more sustainable sources of power. A concrete example is rural Ethiopia, where 70 % of the population lacks reliable access to electricity. Extending the main grid is prohibitively expensive such that mini-grids – localized energy networks – emerge as a cost-effective and dependable solution. They typically consist of small-scale power generation systems and distribution infrastructure which potentially has connection to the main grid. The typical installation includes a back-up diesel generator and utilizes some renewable energy source (RES), for instance photovoltaics or wind, aligning with the goal of decarbonizing electricity. However, the intermittency and uncertainty of RES poses challenges. To mitigate this, batteries are employed. They serve to store excess power when available and provide it during periods of insufficient output from RES [7] as well as to stabilize the mini-grid as they can buffer uncertainties in both generation and consumption.

The integration of a battery energy storage system (BESS) is crucial to address as we navigate towards a sustainable and reliable energy future [16] and investment and replacement costs are of critical concern as we aim at striking a balance between affordability and quality. The concept of second-life lithium-ion batteries (LIBs) emerges as a promising solution: by repurposing LIBs, we can significantly decrease investment costs while simultaneously strengthening sustainability efforts. In this regard, the lifespan of a BESS holds considerable significance. Understanding and optimizing longevity ensures that investments yield lasting benefits, aligning with our sustainability goals. On that account, we aim at operating the BESS in a manner that strikes balance between minimizing degradation alongside operational expenses. Degradation is closely related to the state-of-health (SOH) of a battery. Although there is no uniform definition for the SOH of a battery it still can be quantified in terms of resistance increase and capacity decrease. There are two main aging mechanisms, namely calendar and cycle aging. Calendar aging is the aging mechanism happening when at rest while cycle aging is the aging mechanism happening when in use. During cycle aging, calendar aging still occurs. It is observed that

DOI 10.20347/WIAS.PREPRINT.3125 Berlin 2024

depth-of-discharge (DOD) and temperature both exhibit a significant influence on battery degradation. Higher DODs and higher temperatures lead to faster degradation over time in both capacity and resistance resulting in both capacity and power loss, respectively [3, 18]. Oversizing of a BESS is a viable but very costly solution to prevent high DODs and high temperatures. For this very reason, a battery operation strategy can become key in achieving an optimal trade-off between minimal degradation and optimal operational costs [8]. Thus, tailoring battery operation strategies to the specific demands of the application ensures that LIBs operate optimally and have an extended lifespan.

Another important characteristic of mini-grid management is the presence of uncertainty as naturally introduced by RES, demand and ambient temperature. While these elements can be predicted to some extent, accounting for forecast errors is crucial for a reliable and resilient energy management strategy.

This paper tackles a key challenge in mini-grid operation: handling uncertainties. An energy management strategy for minimizing the daily operational costs of a stand-alone mini-grid under uncertainty is presented. The proposed energy management considers a predefined mini-grid layout and takes into account a prescribed battery (thermal) operation strategy. Building upon this design, a probabilistic optimal control problem (OCP) is set up and solved numerically. The OCP includes state equations describing battery dynamics in form of a coupled ordinary differential equation (ODE) and state constraints, i.e. ranges for battery temperature and state-of-charge (SOC), corresponding to the battery (thermal) operation strategy. Due to the presence of uncertainty such as solar energy, energy demand and ambient temperature, the state constraints become uncertain. As our decisions on optimal dispatch of the mini-grid have to be optimized and applied prior to the realization of uncertainty, it is reasonable to formulate probabilistic state constraints in which a decision is declared to be feasible whenever the random state constraints are satisfied with at least some given probability. Such probabilistic or chance constraints have been introduced in [1] (see also the fundamental monograph [14]). In the context of mini-grids, chance constraints have been considered, for instance, in [9, 23], who investigated the so-called *probability of successful islanding* when, due to a possible outage of the main grid, a mini-grid has to survive in isolated mode for a certain period of time with a given probability. In those papers, the chance constraints were formulated point-wise in time. Though point-wise (or: individual) constraints are easy to deal with at least in the models of these papers, one has to be aware of that pointwise high probability may potentially result in a low probability of satisfying the corresponding constraints over the whole time horizon. Therefore, so-called *joint chance constraints* are preferred in general, but coming at the price of more sophisticated analysis and numerics because of dealing with multivariate distributions.

In a recent paper [11], joint chance constraints were considered in the context of probability of successful islanding of weakly connected mini-grids and the advantages over point-wise constraints became clearly visible. At the same time, in this and many related papers, the battery operation was modeled in quite an elementary manner. The main novelty of the present paper consists in combining joint chance constraints with a more realistic model of battery operation. Mathematically, this leads to the challenge of treating chance constraints in the framework of differential equations.

The paper is organized as follows. Section 2 is dedicated to modeling the power balance, the BESS and the uncertainties. In Section 3 the desired probabilistic OCP will be derived. Section 4 gives details on how to compute probabilities and their derivatives by means of the spherical-radial decomposition. In Section 5 the proposed OCP is solved numerically. Results are given followed by a critical discussion and an outlook.

2 Modeling

2.1 Power balance

The power balance states that power supply and consumption must always be in equilibrium at any time t with power measured in watts (W). It is given in the form of the algebraic equation $P_{in} = P_{out}$. For a stand-alone

mini-grid it reads according to Figure 2.1,

$$\eta_{PV} P_{PV} + \eta_{batt} P^-_{batt} + P_{DG} = P_{load} + \frac{1}{\eta_{batt}} P^+_{batt} + P_{BTMS} + P_{dump} \tag{1}$$

with P_{PV} the photovoltaic (PV) power, P_{DG} the power provided by the back-up diesel generator (DG) and P_{load} the demand. $P_{batt} = P^+_{batt} - P^-_{batt}$ corresponds to battery power with P^+_{batt} the charging and P^-_{batt} the discharging power. The P_{BTMS} represents the power needed by the battery thermal management system (BTMS) for cooling or heating. The model also includes the excess power P_{dump} that has to be dumped if there is a power surplus and the BESS is fully charged. The inverter efficiencies $\eta_{batt}, \eta_{PV} < 1$ are assumed to be constant in this work.

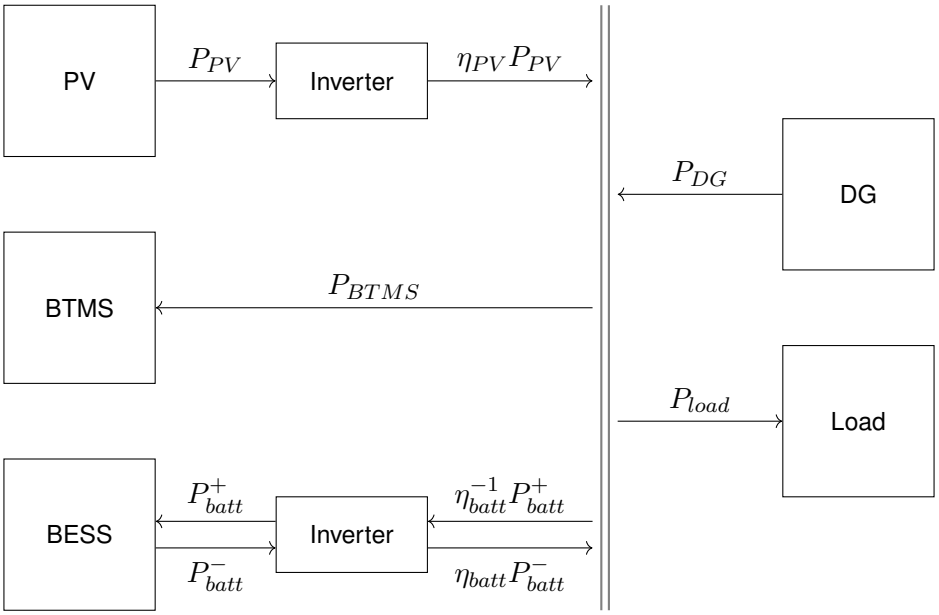

Figure 2.1: A simplified depiction of the installation of a mini-grid and its corresponding power flow. On the left hand-side, the direct current sources and sinks are depicted. On the right hand-side, the alternate current sources and sinks are illustrated. The double-dash line represents the distribution infrastructure where the power balance must hold at any time. The excess power P_{dump} is not part of this illustration but must not be neglected in the power balance.

2.2 Modeling of the battery energy storage system

In the following section, we introduce a model that combines a battery model with a temperature model for a BESS. A BESS consists of several battery packs which, in turn, consist of several battery modules connected in series and parallel. Battery modules are made of battery cells also connected in series and parallel. The exact topology is usually determined by economic and safety considerations and shall not be discussed in this work. Instead, we consider a generic BESS consisting of N battery cells. Electric power is computed as the product of current and voltage, i.e. for a single cell $P_{cell}(t) = V(t) \cdot I(t)$ and for a BESS consisting of N cells

$$P_{batt}(t) = N \cdot P_{cell}(t) = N \cdot V(t) \cdot I(t). \tag{2}$$

We now seek describing equations for the voltage and the current of a battery cell as well as equations describing the dynamics of such a cell.

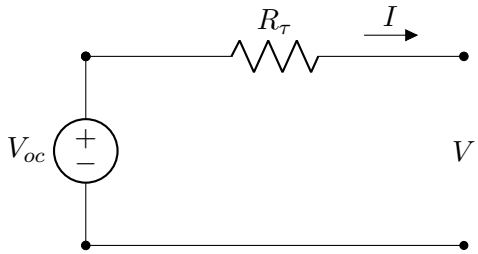

Figure 2.2: 0^{th} order equivalent circuit model

Battery features as e.g. voltage responses, are often and usually approximated using equivalent circuits. An electric circuit serves as an analogue to predict battery's behavior [13]. More precisely, we use a charge reservoir model [13, 17] that defines capacity in units of ampere-hours (Ah). For a day-ahead optimization with a forecast horizon of one day and low time resolution, a 0^{th} order equivalent circuit model (ECM), c.f. Figure 2.2, is appropriate and sufficient [17]. By Kirchhoff's law, see for instance [6], the terminal voltage V, measured in volts (V), is given by

$$V(t) = V_{OC} + R_\tau I(t) \tag{3}$$

with V_{OC} the open-circuit voltage (OCV), R_τ the internal resistance measured in Ohm (Ω) and I the current flowing through the battery measured in ampere (A). We write

$$I(t) = I^+(t) - I^-(t) = \begin{cases} > 0 & \text{for charging} \\ < 0 & \text{for discharging} \end{cases} \qquad I^\pm \geq 0,$$

where we have agreed on the notation $I^+ = \max\{0, I\}$ the positive part and $I^- = \max\{0, -I\}$ the negative part. The OCV is the terminal voltage of the battery when measured at rest, i.e. when the current is zero. The OCV is a function of SOC, SOH and battery temperature. In the following, we will assume $V_{OC} = V_{OC}(SOC)$ as we assume on the one hand the variations w.r.t. to SOH to be small and on the other hand, we operate in a temperature-controlled environment such that we may neglect temperature dependency. From [3], the OCV can be fitted to a function in SOC, c.f. Figure 2.3. The nominal internal resistance R_0 typically is part of the manufacturer's specifications. The progressive increase of resistance over time is one facet of battery degradation. The higher the internal resistance, the higher the voltage drop across the battery such that, eventually, increase in resistance due to degradation translates into power loss. The degraded resistance is denoted by R_τ. The gradual loss of capacity over time is another facet of battery degradation. The capacity of a battery indicates the amount of electric charge that a battery can deliver or store according to the manufacturer's specifications. It is given as the nominal capacity Q_0 measured in ampere-hours for a new battery. In the following, the degraded capacity of a second-life battery will be denoted by Q_τ.

The SOC is quantified as the ratio of available capacity and degraded (total) capacity. The SOC of a 0^{th} order ECM can be modeled by means of Coulomb counting, i.e. integrating the current over time.

$$SOC(t) = \frac{Q(t)}{Q_\tau} = SOC(t_0) + \int_{t_0}^{t} \frac{I(s)}{Q_\tau}\, ds.$$

This yields the dynamics for the SOC,

$$Q_\tau SOC'(t) = I(t) = \text{C-rate} \cdot \frac{Q_0}{1\,\mathrm{h}}. \tag{4}$$

At this point, the C-rate has been introduced, too. The C-rate quantifies the rate at which a battery is charged or discharged in relation to its nominal capacity and is defined as the inverse of the time it takes, in hours (h), to fully discharge a battery.

Given the 0^{th} order ECM, equations for the battery temperature evolution can be set up by means of Newton's law of cooling yielding an ODE, see for instance [17]. The temperature of a battery is a function of heat generated

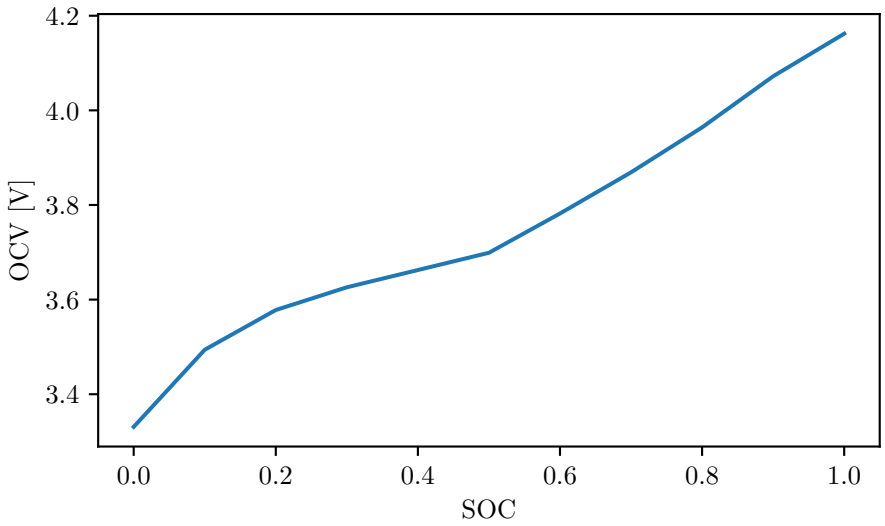

Figure 2.3: Open-circuit voltage as a function of state-of-charge

by the battery through operation and the heat exchange between the battery and its environment and typically is given in units of Kelvin (K). For the considered 0^{th} order ECM, the heat generated by the battery that is taken into account is the Joule heating. Heat is generated (or consumed) in further ways, which will be neglected in the following as they are comparably small [17]. The rate at which heat is transferred through a material is given by [6]

$$\frac{\lambda A}{l}\Delta T = UA\Delta T$$

with l, given in meters (m), representing material thickness, λ measured in $\mathrm{W/m \cdot K}$ the thermal conductivity and A the exposed material surface area (the "interface") given in units of m^2. Eventually, we call U the thermal transmittance which is given in units of $\mathrm{W/m^2 \cdot K}$.

In a mini-grid application, several battery packs are stored in an enclosure. This means that there must be a separation of the weather-dependent environment and the actual environment the batteries are operating in. We thus seek a coupled ODE describing battery cell and battery enclosure temperature. To regulate the battery cell temperature, we introduce a BTMS. Denote T_{cell} the battery cell temperature, T_{en} the enclosure temperature and T_{amb} the ambient temperature. The battery temperature then evolves, by Newton's law of cooling, according to the following coupled ODE,

$$C_{cell}T'_{cell}(t) = R_\tau I^2 + U_{cell}\big(T_{en} - T_{cell}\big) \tag{5a}$$
$$C_{en}T'_{en}(t) = \eta_{BTMS}P_{BTMS} + N \cdot U_{cell}\big(T_{cell} - T_{en}\big) + U_{en}\big(T_{amb} - T_{en}\big) \tag{5b}$$

with $Q_{BTMS} = \eta_{BTMS}P_{BTMS}$ the thermal power given as a fraction of the electric power P_{BTMS} needed for cooling. This approach assumes a constant air velocity and can be further developed by adding a fan and a heat exchanger. C_{cell}, C_{en} are the battery and enclosure heat capacity, respectively, while U_{cell}, U_{en} denote their battery and enclosure thermal conductances. N refers to the number of battery cells the BESS consists of.

In this work, a high energy 18650 lithium-ion cylindrical battery cell manufactured by Sanyo, labeled UR18650E has been considered. The cell specifications according to the data sheet as well as some thermodynamic properties are summarized in Table 2.1. Some thermodynamic parameters of the battery enclosure are listed in Table 2.2. Note that the thermodynamic parameters are not meant to represent a specific enclosure topology. Instead, we assume that the BESS consists of well-insulating materials.

Table 2.1: Cell specification and thermodynamic properties

Description	Symbol	Value
Nominal capacity	Q_0	$2.05\ \mathrm{Ah}$
Battery specific heat capacity	c_{cell}	$890\ \mathrm{J/kg \cdot K}$ [4]
Battery thermal transmittance	λ_{cell}	$0.2\ \mathrm{W/m \cdot K}$ [2]

Table 2.2: Thermodynamic properties of battery enclosure

Description	Symbol	Value
Enclosure heat capacity	C_{en}	$63\ \mathrm{kJ/W}$ [17]
Enclosure thermal conductance	U_{en}	$0.45\ \mathrm{W/m^2 \cdot K}$

2.3 Modeling the uncertainties

For a day-ahead optimization, we consider uncertainties in the forecasts of PV power, demand and and ambient temperature. Using historical data, future values are forecasted coming at the price of prediction errors. We thus represent $x_t = \hat{x}_t + \xi_t$, where $\hat{x}_t$ corresponds to the deterministic forecast and ξ_t to the uncertain prediction error.

Causal and invertible ARMA(p, q) processes can be forecasted up to some prediction error [19]. A time series $\{x_t\}_t$ is called an ARMA(p, q) process if $x_t + \sum_{j=1}^{p} \phi_j x_{t-j} = \omega_t + \sum_{j=1}^{q} \theta_j \omega_{t-j}$ where $\omega_t \sim$ iid $\mathcal{N}(0, \sigma_\omega^2)$. An ARMA$(p, q)$ model is said to be causal if $x_t = \sum_{j=0}^{\infty} \psi_j \omega_{t-j}$, $\psi_0 = 1$ with $\sum_{j=0}^{\infty} |\psi_j| < \infty$. The ψ-weights of a causal ARMA(p, q) process satisfy

$$\begin{cases} \psi_j + \sum_{k=1}^{p} \phi_k \psi_{j-k} = 0 & \text{if } j \geq \max(p, q+1) \\ \psi_j + \sum_{k=1}^{p} \phi_k \psi_{j-k} = \theta_j & \text{if } 0 \leq j \leq \max(p, q+1). \end{cases} \tag{6}$$

An ARMA(p, q) model is said to be invertible if $\omega_t = \sum_{j=0}^{\infty} \pi_j x_{t-j}$, $\pi_0 = 1$ with $\sum_{j=0}^{\infty} |\pi_j| < \infty$ and the π-weights of an invertible ARMA(p, q) satisfy an analogue to Equation (6).

Let $\{x_t\}_t$ be a causal and invertible ARMA(p, q) process. Assume there exists a complete history of measurements $\{x_0, x_{-1}, x_{-2}, \dots\}$. It holds $x_t = \hat{x}_t + \xi_t$ with $\hat{x}_t$ the prediction and ξ_t the prediction error. More precisely,

$$\hat{x}_t = -\sum_{j=1}^{t-1} \pi_j \hat{x}_{t-j} - \sum_{j=t}^{\infty} \pi_j x_{t-j}$$
$$\xi_t = \sum_{j=0}^{t-1} \psi_j \omega_{t-j}$$

and the prediction errors are correlated with $\mathrm{cov}(\xi_t, \xi_{t+m}) = \mathbb{E}\big(\xi_t \xi_{t+m}\big) = \sigma_\omega^2 \sum_{j=0}^{m-1} \psi_j \psi_{j+m}$.

3 Optimal control formulation

Given a battery and a battery temperature model, a probabilistic OCP that aims at minimizing the daily operational costs subject to a battery (thermal) operation strategy will be proposed. The probabilistic OCP takes into account the uncertainties introduced by PV power, demand and ambient temperature, yielding a reliable energy management strategy. We proceed in the following manner. In a first step, a deterministic OCP for minimizing the daily operational costs of an isolated mini-grid will be introduced. In a second step, it will be discussed how

one can deal with the uncertainties and the approach taken in this work will be described. In a last step, the discretized OCP considered in this work will be established.

The operational costs of a stand-alone mini-grid are determined by fuel consumption of the back-up DG, mitigating financial expenses as well as environmental impact. Without knowledge of the exact DG, we decide to minimize the total DG power. Motivated by the fact that excess power is undesirable as it can affect the stability of a mini-grid, c.f. [15], one could also consider penalizing dumping excess power.

3.1 Deterministic problem formulation

For a day-ahead optimization the goal is to find an optimal energy management strategy that minimizes the operational costs. In the off-grid case, this translates into minimizing diesel fuel consumption. The optimization is subject to the algebraic power balance (1), subject to a battery model (2), (3) and (4), and temperature model (5) and subject to SOC and battery temperature constraints corresponding to the battery operation strategy. Before proceeding, we need to decide on control variables. One obvious control variable is the cooling power P_{BTMS}. Battery systems can respond quickly to fluctuations in both supply and demand, making them ideal for managing short-term variations and uncertainties in PV generation and load. Conversely, a DG is better suited for providing power over longer periods rather than handling rapid changes. Thus, the variables declared as controls are the DG power P_{DG} and the excess power P_{excess}. Battery power adjusts accordingly. Rearranging the power balance, Equation (1), yields

$$\begin{aligned} \eta_{batt}^{-1} P_{batt}^{+} - \eta_{batt} P_{batt}^{-} &= \eta_{PV}\hat{P}_{PV} + P_{DG} - \hat{P}_{load} - P_{BTMS} - P_{dump} =: P_{\text{brutto}} \\ \iff \quad P_{batt} = P_{batt}^{+} - P_{batt}^{-} &= \eta_{batt} \max\{0, P_{\text{brutto}}\} - \eta_{batt}^{-1} \max\{0, -P_{\text{brutto}}\} =: P_{\text{netto}} \end{aligned} \tag{7}$$

The equivalence follows due to the easy observation $P_{\text{brutto}} = \max\{0, P_{\text{brutto}}\} - \max\{0, -P_{\text{brutto}}\}$. On the other hand, it holds

$$P_{batt} = NP_{cell} = N(V \cdot I) = N\big(V_{oc} + R_\tau I\big)I = N\big(V_{oc}I + R_\tau I^2\big). \tag{8}$$

Combining Equation (7) and Equation (8) eventually yields an expression for the current I,

$$2R_\tau I = -V_{oc} + \sqrt{V_{oc}^2 + 4R_\tau N^{-1} P_{\text{netto}}}.$$

The OCP taken into considerations reads as follows. Minimize the DG fuel consumption subject to state equations, and subject to state and final state constraints outlined in the battery operation strategy. The final state constraints (or cycling constraints) are imposed in order to ensure that tomorrow's energy management does not come at the expense of the energy management of the day after tomorrow. More precisely,

$$\min \quad \int_{t_0}^{t_f} P_{DG}(t)\, dt \tag{9a}$$

$$\text{s.t.} \quad SOC'(t) = \frac{-V_{oc} + \sqrt{V_{oc}^2 + 4R_\tau N^{-1} P_{\text{netto}}}}{2R_\tau Q_\tau} \tag{9b}$$

$$C_{cell} T'_{cell}(t) = R_\tau I^2 + U_{cell}\big(T_{en} - T_{cell}\big) \tag{9c}$$

$$C_{en} T'_{en}(t) = \eta_{BTMS} P_{BTMS} + N \cdot U_{cell}\big(T_{cell} - T_{en}\big) + U_{en}\big(T_{amb} - T_{en}\big) \tag{9d}$$

$$SOC(t) \in [SOC^{\min}, SOC^{\max}] \quad \forall t \in [t_0, t_f] \tag{9e}$$

$$T_{cell}(t) \in [T^{\min}, T^{\max}] \quad \forall t \in [t_0, t_f] \tag{9f}$$

$$SOC(t_f) \geq SOC_f \tag{9g}$$

$$T_{cell}(t_f) \leq T_f \tag{9h}$$

We denote $\boldsymbol{u} = (\boldsymbol{u}^{(1)}, \boldsymbol{u}^{(2)}, \boldsymbol{u}^3)^T = (P_{BTMS}, P_{DG}, P_{dump})^T$ the control variable and $\boldsymbol{x} = (\boldsymbol{x}^{(1)}, \boldsymbol{x}^{(2)}, \boldsymbol{x}^{(3)})^T = (SOC, T_{cell}, T_{en})^T$ the state variable. Accordingly, the OCP reads,

$$\begin{aligned} \min_{\boldsymbol{u}} \quad & J(\boldsymbol{u}) = \int_{t_0}^{t_f} \boldsymbol{u}^{(2)}(t)\, dt \\ \text{s.t.} \quad & \frac{d\boldsymbol{x}(t;\boldsymbol{u})}{dt} = F(t,\boldsymbol{x},\boldsymbol{u}) = A\boldsymbol{x} + f(t,\boldsymbol{x},\boldsymbol{u}) \\ & \boldsymbol{x}^{(i)}(t;\boldsymbol{u}) \in [x^{(i)}_{\min}, x^{(i)}_{\max}] \quad \forall t \in [t_0,t_f], \qquad i = 1,2 \\ & \boldsymbol{x}^{(1)}(t_f;\boldsymbol{u}) \geq x_f^{(1)} \\ & \boldsymbol{x}^{(2)}(t_f;\boldsymbol{u}) \leq x_f^{(2)} \end{aligned}$$

with

$$A = \begin{pmatrix} 0 & 0 & 0 \\ 0 & -\frac{U_{cell}}{C_{cell}} & \frac{U_{cell}}{C_{cell}} \\ 0 & \frac{N\cdot U_{cell}}{C_{en}} & -\frac{N\cdot U_{cell}}{C_{en}} - \frac{U_{en}}{C_{en}} \end{pmatrix} \quad \text{and} \quad f(t,\boldsymbol{x},\boldsymbol{u}) = \begin{pmatrix} Q_\tau^{-1} I(t;\boldsymbol{x}^{(1)},\boldsymbol{u}) \\ \frac{R_\tau}{C_{cell}} I^2(t;\boldsymbol{x}^{(1)},\boldsymbol{u}) \\ \frac{\eta_{BTMS}\boldsymbol{u}^{(1)}}{C_{en}} + \frac{U_{en}}{C_{en}} T_{amb}(t) \end{pmatrix}$$

Remark. 1 A battery operation strategy not only asks for SOC and temperature management but also for keeping voltage and current bounded. This is not explicitly included in this work as a consequence of a mini-grid being a low C-rate application resulting in rather low currents and restricting diesel usage. Choosing the interval $[SOC^{\min}, SOC^{\max}]$ in (4) suitably justifies dropping bounds for the voltage, too.

2 Including a back-up DG asks for the binary decision of switching on and off the generator. This is neglected in this undertaking. The reader is referred to e.g. [12].

3.2 Probabilistic problem formulation

Recall the uncertainties PV power P_{PV}, demand P_{load} and ambient temperature T_{amb}. Denote by ξ the uncertainty. By choice of the control variables, it follows $P_{\text{brutto}} = P_{\text{brutto}}(t;\boldsymbol{u},\xi)$ yielding $I = I(t;\boldsymbol{x}^{(1)},\boldsymbol{u},\xi)$. This immediately gives that the uncertainty in the forecasts of solar power and demand translate into uncertainty in the battery SOC dynamics. Similarly, battery temperature becomes uncertain. With a slight abuse of notation, we write

$$\frac{d\boldsymbol{x}(t;\boldsymbol{u},\xi)}{dt} \quad = \quad F(t;\boldsymbol{x},\boldsymbol{u},\xi)$$

and the state constraints have to take another form for which several possibilities exist. A pretty cheap but not very robust solution is to ask the state to stay bounded in expectation. In contrast, a very robust but also very expensive formulation is to ask the state to stay bounded for every possible realization of the uncertainty. As a good and fair trade-off between robustness and costs, a probabilistic constraint comes into play: we ask the state variable to stay bounded with a given, prescribed probability level (PL). This is the path we will take in this work. To be exact,

$$\min_{\boldsymbol{u}} \quad J(\boldsymbol{u}) = \int_{t_0}^{t_f} \boldsymbol{u}^{(2)}(t)\, dt$$

subject to the state equations

$$\begin{aligned} \frac{d\boldsymbol{x}(t;\boldsymbol{u},\xi)}{dt} \quad &= \quad F(t;\boldsymbol{x},\boldsymbol{u},\xi) \\ &= \quad A\boldsymbol{x} + f(t;\boldsymbol{x},\boldsymbol{u},\xi) \end{aligned}$$

with

$$A = \begin{pmatrix} 0 & 0 & 0 \\ 0 & -\frac{U_{cell}}{C_{cell}} & \frac{U_{cell}}{C_{cell}} \\ 0 & \frac{N \cdot U_{cell}}{C_{en}} & -\frac{N \cdot U_{cell}}{C_{en}} - \frac{U_{en}}{C_{en}} \end{pmatrix} \quad \text{and} \quad f(t; \boldsymbol{x}, \boldsymbol{u}, \xi) = \begin{pmatrix} \frac{1}{Q_\tau} I(t; \boldsymbol{x}^{(1)}, \boldsymbol{u}, \xi) \\ \frac{R_\tau}{C_{cell}} I^2(t; \boldsymbol{x}^{(1)}, \boldsymbol{u}, \xi) \\ \frac{\eta_{BTMS} \boldsymbol{u}^{(1)}}{C_{en}} + \frac{U_{en}}{C_{en}} T_{amb}(t; \xi) \end{pmatrix}$$

subject to the joint chance constraints (JCCs)

$$\mathbb{P}\big(\boldsymbol{x}^{(i)}(t; \boldsymbol{u}, \xi) \in [x^{(i)}_{\min}, x^{(i)}_{\max}] \quad \forall t \in [t_0, t_f]\big) \quad \geq \quad p_i, \qquad i = 1, 2$$

and subject to the cycling chance constraints (CCCs)

$$\begin{aligned} \mathbb{P}\big(\boldsymbol{x}^{(1)}(t_f; \boldsymbol{u}, \xi) \geq x^{(1)}_f\big) \quad &\geq \quad q_1 \\ \mathbb{P}\big(\boldsymbol{x}^{(2)}(t_f; \boldsymbol{u}, \xi) \leq x^{(2)}_f\big) \quad &\geq \quad q_2 \end{aligned}$$

3.3 Discretized problem formulation

The approach taken is a first-discretize-then-optimize approach. Therefore, in a first step, a discretization scheme is chosen. Using this discretization, the above ODEs are solved using an implicit Euler scheme. Eventually, the calculation of the gradients of the output equations are discussed. For readability, set

$$\Xi(t; \xi) \coloneqq \big(P_{PV}(t; \xi), P_{load}(t; \xi), T_{amb}(t; \xi)\big)^T.$$

Let $\{t_0, t_1, \ldots, t_K = t_f\}$ be an equidistant discretization of the time horizon with $t_k = t_0 + \frac{t_f - t_0}{K} k$, $k = 1, \ldots, K$. For readability, again, set

$$\begin{aligned} \boldsymbol{u}_k &= \boldsymbol{u}(t_k) \\ \Xi_k &= \Xi(t_k; \xi) \\ \boldsymbol{x}_k &= \boldsymbol{x}(t_k). \end{aligned}$$

By implicit Euler scheme, the discretized state equations read

$$\begin{aligned} \boldsymbol{x}_{k+1} &= \boldsymbol{x}_k + \Delta t \Big(A \boldsymbol{x}_{k+1} + f\big(t_{k+1}, \boldsymbol{x}_{k+1}, \boldsymbol{u}_{k+1}, \Xi_{k+1}\big) \Big), \\ &= \boldsymbol{x}_k + \Delta t \Big(A \boldsymbol{x}_{k+1} + \hat{f}\big(t_{k+1} \boldsymbol{u}_{k+1}, I(\boldsymbol{x}^{(1)}_{k+1}, \boldsymbol{u}_{k+1}, \Xi_{k+1}), \Xi_{k+1}\big) \Big), \qquad k = 0, \ldots, K-1. \end{aligned}$$

Next, we introduce the indices $\hat{K}^{(i)} = \text{argmax}_k \boldsymbol{x}^{(i)}_k$ and $\hat{k}^{(i)} = \text{argmin}_k \boldsymbol{x}^{(i)}_k$. It holds for $i = 1, 2$,

$$\begin{aligned} & \boldsymbol{x}^{(i)}_k \in [\boldsymbol{x}^{(i)}_{\min}, \boldsymbol{x}^{(i)}_{\max}] \quad \forall k = 0, \ldots, K \\ \iff \quad & \max_k \boldsymbol{x}^{(i)}_k - x^{(i)}_{\max} \leq 0 \quad \text{and} \quad x^{(i)}_{\min} - \min_k \boldsymbol{x}^{(i)}_k \leq 0 \\ \iff \quad & \max \big\{ \, \boldsymbol{x}^{(i)}_{\hat{K}^{(i)}} - x^{(i)}_{\max}, \quad x^{(i)}_{\min} - \boldsymbol{x}^{(i)}_{\hat{k}^{(i)}} \, \big\} \leq 0. \end{aligned}$$

Denote

$$\begin{aligned} g^{(i)}(\boldsymbol{u}, \xi) &= \max \big\{ \boldsymbol{x}^{(i)}_{\hat{K}^{(i)}} - x^{(i)}_{\max}, x^{(i)}_{\min} - \boldsymbol{x}^{(i)}_{\hat{k}^{(i)}} \big\}, \qquad i = 1, 2 \\ h^{(1)}(\boldsymbol{u}, \xi) &= x^{(1)}_f - \boldsymbol{x}^{(1)}_K \\ h^{(2)}(\boldsymbol{u}, \xi) &= \boldsymbol{x}^{(2)}_K - x^{(2)}_f \end{aligned}$$

such that the discretized output equations read

$$\begin{aligned} \varphi^{(i)}(\boldsymbol{u}) &= \mathbb{P}\big(g^{(i)}(\boldsymbol{u}, \xi) \leq 0\big) \geq p_i, \quad i = 1, 2 \\ \gamma^{(i)}(\boldsymbol{u}) &= \mathbb{P}\big(h^{(i)}(\boldsymbol{u}, \xi) \leq 0\big) \geq q_i, \quad i = 1, 2. \end{aligned}$$

4 Spherical-radial decomposition

How can we compute the above probabilities and, within an optimization framework, determine their derivatives? One effective approach is the spherical-radial decomposition.

For a centered m-dimensional Gaussian random vector $\xi \sim \mathcal{N}(0, \Sigma)$ the so-called spherical-radial decomposition $\xi = \eta L \zeta$ with $\eta \sim \chi(m)$ (one-dimensional Chi-distribution with m degrees of freedom), $\zeta \sim \mathcal{U}(\mathbb{S}^{m-1})$ (uniform distribution on unit sphere) and L such that $LL^T = \Sigma$ holds true. This implies that the Gaussian probability of a measurable set $M \subseteq \mathbb{R}^m$ may be represented as the spherical integral

$$\int_{v \in \mathbb{S}^{m-1}} \mu_\eta \left(\{ r \geq 0 \mid rLv \in M \} \right) \, d\mu_\zeta(v).$$

Applied to a set defined as an inequality $M = \{ z \in \mathbb{R}^m \mid g(u,z) \leq 0 \}$ (where u can be interpreted as a fixed control), this yields that

$$\varphi(u) := \mathbb{P} \left(g(u, \xi) \leq 0 \right) = \int_{v \in \mathbb{S}^{m-1}} \mu_\eta \left(\{ r \geq 0 \mid g(u, rLv) \leq 0 \} \right) \, d\mu_\zeta(v).$$

If g is regular enough, meaning that it is continuous and for each $v \in \mathbb{S}^{m-1}$ the ray $\{ rLv \mid r \geq 0 \}$ enters or leaves the set $\{ z \in \mathbb{R}^m \mid g(u,z) \leq 0 \}$ only for a finite number $n^{u,v}$ of times, this probability can be specified as

$$\varphi(u) = \int_{v \in \mathbb{S}^{m-1}} \sum_{i=1}^{n^{u,v}} \mu_\eta \left([r_i(u,v), R_i(u,v)] \right) \, d\mu_\zeta(v) \tag{10a}$$

$$= \int_{v \in \mathbb{S}^{m-1}} \sum_{i=1}^{n^{u,v}} \Big[F_\eta\big(R_i(u,v)\big) - F_\eta\big(r_i(u,v)\big) \Big] \, d\mu_\zeta(v). \tag{10b}$$

Here, r_1 is defined to be the smallest $r \geq 0$ such that $g(u, rLv) \leq 0$. Accordingly, the $[r_i(u,v), R_i(u,v)]$ are the disjoint intervals describing the intersection of the ray $\{ rLv \mid r \geq 0 \}$ with the closed set $\{ z \in \mathbb{R}^m \mid g(u,z) \leq 0 \}$. Note, that the last such interval could be unbounded, hence $R_{n^{u,v}}(u,v) = \infty$ is possible. In the last formula, F_η denotes the cumulative distribution function of the one-dimensional Chi-distribution with m degrees of freedom. Determining the Gaussian probability of a set in this way rather than by crude Monte Carlo simulation provides estimates with possibly significantly reduced variance [5, Table 1], [20, Eq. (1.5)]. The numerical approximation of the spherical integral involved would result in turning into a finite sum according to an efficient uniform sampling of the unit sphere and by averaging this sum.

If it comes to optimization subject to the chance constraint $\varphi(u) \geq 0$, then at least first order information about φ should be available. Differentiability of φ is a delicate issue even in case that all input data of the problem are differentiable. In particular, g will be supposed to be differentiable. More precisely, growth conditions and certain constraint qualifications have to be satisfied (see, e.g., [21]). These would then allow one to interchange differentiation and integration in (10):

$$\nabla \varphi(u) = \int_{v \in \mathbb{S}^{m-1}} \sum_{i=1}^{n^{u,v}} \Big[F_\eta'(R_i(u,v)) \nabla_u R_i(u,v) - F_\eta'\big(r_i(u,v)\big) \nabla_u R_i(u,v) \Big] \, d\mu_\zeta(v), \tag{11}$$

where we exploited that the distribution function F_η is differentiable with derivative $F_\eta'(t) = f_\eta(t)$ and f_η being the probability density of the Chi-distribution with m degrees of freedom. Appropriate conditions would also guarantee that the endpoint functions $r_i(u,v), R_i(u,v)$ of the intervals considered above are differentiable with gradients computable via the implicit function theorem. One would then obtain the gradient formulae

$$\nabla_u (r_i/R_i)(u,v) = \frac{\nabla_u g(u, (r_i/R_i)Lv)}{\langle \nabla_z g(u, (r_i/R_i)Lv), Lv \rangle} \quad (i = 1, \ldots, n^{u,v}).$$

Altogether, this yields the gradient formula

$$\nabla\varphi(u) = \int_{v\in\mathbb{S}^{m-1}} \sum_{i=1}^{n^{u,v}} \Big[f_\eta\big(R_i(u,v)\big) \left(\frac{\nabla_u g(u, R_i L v)}{\langle \nabla_z g(u, R_i L v), Lv\rangle} \right) - f_\eta\big(r_i(u,v)\big) \left(\frac{\nabla_u g(u, r_i L v)}{\langle \nabla_z g(u, r_i L v), Lv\rangle} \right) d\mu_\zeta(v).$$

As can be seen from the latter equation, for this purpose gradients w.r.t. u and ξ have to be computed.

In order to compute the gradient of the individual state variables w.r.t. the control variables, one derives the Jacobian $\frac{\partial \boldsymbol{x}_{m^*}}{\partial \boldsymbol{u}^{(i)}} \in \mathbb{R}^{3\times K}$, $i \in \{1,2,3\}$. The gradient is computed using the implicit Euler scheme. For readability set

$$\begin{aligned} I_k &= I(t_k, \boldsymbol{x}_k^{(1)}, \boldsymbol{u}_k, \Xi_k), \\ \hat{f}_k &= \hat{f}\big(t_k, \boldsymbol{u}_k, I_k, \Xi_k\big). \end{aligned}$$

Using the implicit Euler scheme, one computes for $k \in \{1,\dots,K\}$ fixed, $i \in \{1,2,3\}$, $l \le k$,

$$\begin{aligned} \frac{\partial \boldsymbol{x}_k}{\partial \boldsymbol{u}_l^{(i)}} &= \frac{\partial \boldsymbol{x}_{k-1}}{\partial \boldsymbol{u}_l^{(i)}} + \Delta t \left(A \frac{\partial \boldsymbol{x}_k}{\partial \boldsymbol{u}_l^{(i)}} + \frac{\partial \hat{f}_k}{\partial \boldsymbol{u}_l^{(i)}} \right) \\ &= \frac{\partial \boldsymbol{x}_{k-1}}{\partial \boldsymbol{u}_l^{(i)}} + \Delta t \left(A \frac{\partial \boldsymbol{x}_k}{\partial \boldsymbol{u}_l^{(i)}} + \frac{\partial \hat{f}_k}{\partial \boldsymbol{u}_k^{(i)}} \frac{\partial \boldsymbol{u}_k^{(i)}}{\partial \boldsymbol{u}_l^{(i)}} + \frac{\partial \hat{f}_k}{\partial I_k} \frac{\partial I_k}{\partial \boldsymbol{u}_l^{(i)}} \right) \\ &= \frac{\partial \boldsymbol{x}_{k-1}}{\partial \boldsymbol{u}_l^{(i)}} + \Delta t \left(A \frac{\partial \boldsymbol{x}_k}{\partial \boldsymbol{u}_l^{(i)}} + \frac{\partial \hat{f}_k}{\partial \boldsymbol{u}_k^{(i)}} \frac{\partial \boldsymbol{u}_k^{(i)}}{\partial \boldsymbol{u}_l^{(i)}} + \frac{\partial \hat{f}_k}{\partial I_k} \left[\frac{\partial I_k}{\partial \boldsymbol{x}_k} \frac{\partial \boldsymbol{x}_k}{\partial \boldsymbol{u}_l^{(i)}} + \frac{\partial I_k}{\partial \boldsymbol{u}_k^{(i)}} \frac{\partial \boldsymbol{u}_k^{(i)}}{\partial \boldsymbol{u}_l^{(i)}} \right] \right) \end{aligned}$$

giving

$$\left(I - \Delta t \left[A + \frac{\partial \hat{f}_k}{\partial I_k} \frac{\partial I_k}{\partial \boldsymbol{x}_k} \right] \right) \frac{\partial \boldsymbol{x}_k}{\partial \boldsymbol{u}_l^{(i)}} = \frac{\partial \boldsymbol{x}_{k-1}}{\partial \boldsymbol{u}_l^{(i)}} + \Delta t \left[\frac{\partial \hat{f}_k}{\partial \boldsymbol{u}_k^{(i)}} + \frac{\partial \hat{f}_k}{\partial I_k} \frac{\partial I_k}{\partial \boldsymbol{u}_k^{(i)}} \right] \delta_{k,l}$$

eventually yielding Algorithm 4.1.

As before, to compute the gradient w.r.t. the uncertainties, one derives the Jacobian $\frac{\partial \boldsymbol{x}_{m^*}}{\partial \xi} \in \mathbb{R}^{3\times m}$ and then restricts to the respective row yielding. Again, one computes the gradient w.r.t. ξ using the implicit Euler scheme. For $k \in \{1,\dots,K\}$ fixed

$$\begin{aligned} \frac{\partial \boldsymbol{x}_k}{\partial \xi} &= \frac{\partial \boldsymbol{x}_{k-1}}{\partial \xi} + \Delta t \left(A \frac{\partial \boldsymbol{x}_k}{\partial \xi} + \frac{\partial \hat{f}_k}{\partial \xi} \right) \\ &= \frac{\partial \boldsymbol{x}_{k-1}}{\partial \xi} + \Delta t \left(A \frac{\partial \boldsymbol{x}_k}{\partial \xi} + \frac{\partial \hat{f}_k}{\partial \Xi_k} \frac{\partial \Xi_k}{\partial \xi} + \frac{\partial \hat{f}_k}{\partial I_k} \frac{\partial I_k}{\partial \xi} \right) \\ &= \frac{\partial \boldsymbol{x}_{k-1}}{\partial \xi} + \Delta t \left(A \frac{\partial \boldsymbol{x}_k}{\partial \xi} + \frac{\partial \hat{f}_k}{\partial \Xi_k} \frac{\partial \Xi_k}{\partial \xi} + \frac{\partial \hat{f}_k}{\partial I_k} \left[\frac{\partial I_k}{\partial \boldsymbol{x}_k} \frac{\partial \boldsymbol{x}_k}{\partial \xi} + \frac{\partial I_k}{\partial \Xi_k} \frac{\partial \Xi_k}{\partial \xi} \right] \right) \end{aligned}$$

giving

$$\left(I - \left[\Delta t A + \frac{\partial \hat{f}_k}{\partial I_k} \frac{\partial I_k}{\partial \boldsymbol{x_k}} \right] \right) \frac{\partial \boldsymbol{x}_k}{\partial \xi} = \frac{\partial \boldsymbol{x}_{k-1}}{\partial \xi} + \Delta t \left(\frac{\partial \hat{f}_k}{\partial \Xi_k} \frac{\partial \Xi_k}{\partial \xi} + \frac{\partial \hat{f}_k}{\partial I_k} \frac{\partial I_k}{\partial \Xi_k} \frac{\partial \Xi_k}{\partial \xi} \right)$$

eventually yielding Algorithm 4.2.

Algorithm 4.1: Computation of $\frac{\partial \boldsymbol{x}_{m^*}}{\partial \boldsymbol{u}^{(i)}}$

for $l = 1, \dots, K$ **do**
  if $l \leq m^*$ **then**
    Compute $\frac{\partial \boldsymbol{x}_l}{\partial \boldsymbol{u}_l^{(i)}}$ by solving

$$\left(I - \Delta t\left[A + \frac{\partial \hat{f}_l}{\partial I_l}\frac{\partial I_l}{\partial \boldsymbol{x}_l}\right]\right)\frac{\partial \boldsymbol{x}_l}{\partial \boldsymbol{u}_l^{(i)}} = \Delta t\left[\frac{\partial \hat{f}_l}{\partial \boldsymbol{u}_l^{(i)}} + \frac{\partial \hat{f}_l}{\partial I_l}\frac{\partial I_l}{\partial \boldsymbol{u}_l^{(i)}}\right]$$

    for $k = l+1, \dots, m^*$ **do**
      Compute $\frac{\partial \boldsymbol{x}_k}{\partial \boldsymbol{u}_l^{(i)}}$ by solving

$$\left(I - \Delta t\left[A + \frac{\partial \hat{f}_k}{\partial I_k}\frac{\partial I_k}{\partial \boldsymbol{x}_k}\right]\right)\frac{\partial \boldsymbol{x}_k}{\partial \boldsymbol{u}_l^{(i)}} = \frac{\partial \boldsymbol{x}_{k-1}}{\partial \boldsymbol{u}_l^{(i)}}$$

    return $\frac{\partial x_{m^*}}{\partial u_l^{(i)}}$
  else
    return $\frac{\partial \boldsymbol{x}_{m^*}}{\partial u_l^{(i)}} = 0$;
return $\frac{\partial \boldsymbol{x}_{m^*}}{\partial \boldsymbol{u}^{(i)}} = \left(\frac{\partial \boldsymbol{x}_{m^*}}{\partial \boldsymbol{u}_1^{(i)}}, \frac{\partial \boldsymbol{x}_{m^*}}{\partial \boldsymbol{u}_2^{(i)}}, \dots, \frac{\partial \boldsymbol{x}_{m^*}}{\partial \boldsymbol{u}_K^{(i)}}\right)^T \in \mathbb{R}^{3\times K}$

Algorithm 4.2: Computation of $\frac{\partial \boldsymbol{x}_{m^*}}{\partial \xi}$

Set $\frac{\partial \boldsymbol{x}_0}{\partial \xi} = 0 \in \mathbb{R}^{3\times m}$. ;
for $k = 1, \dots, m^*$ **do**
  Compute $\frac{\partial \boldsymbol{x}_k}{\partial \xi}$ by solving

$$\left(I - \left[\Delta t A + \frac{\partial \hat{f}_k}{\partial I_k}\frac{\partial I_k}{\partial \boldsymbol{x_k}}\right]\right)\frac{\partial \boldsymbol{x}_k}{\partial \xi} = \frac{\partial \boldsymbol{x}_{k-1}}{\partial \xi} + \Delta t\left(\frac{\partial \hat{f}_k}{\partial \Xi_k}\frac{\partial \Xi_k}{\partial \xi} + \frac{\partial \hat{f}_k}{\partial I_k}\frac{\partial I_k}{\partial \Xi_k}\frac{\partial \Xi_k}{\partial \xi}\right)$$

return $\frac{\partial \boldsymbol{x}_{m^*}}{\partial \xi} \in \mathbb{R}^{3\times m}$

Remark. In [20], as mentioned above, in order to make use of the gradient formula (11) enough regularity is presumed. More precisely, convexity in the uncertainty, i.e. in the second argument, of the function g is assumed. In addition, the function g is clearly assumed to be differentiable. This holds not true in our case. Nonetheless, we exploit the gradient formula for performing numerical computations.

5 Numerical results

In a very first step, the mini-grid design has to be determined. Special attention should be paid to the integration of BESS, its sizing and its operation strategy. In a second step, the uncertainties are introduced. Eventually, the results will be presented and discussed critically with a focus on the lack of systematic methodology for sizing and corresponding room for improvement in order to ensure optimal performance.

Given a demand profile, PV output power can be scaled such that, integrated over time, they are roughly equal. After having decided on a battery operation strategy and having at hand demand and PV power profiles, the

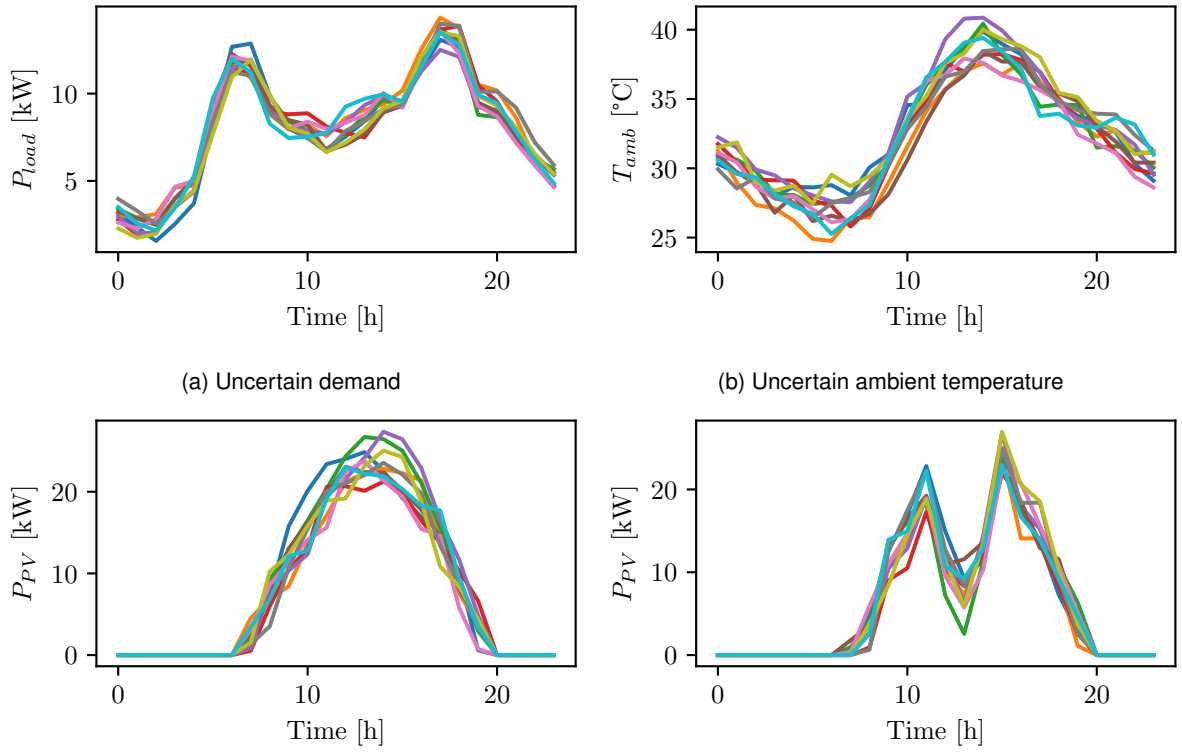

(a) Uncertain demand

(b) Uncertain ambient temperature

(c) Uncertain PV power on a sunny day

(d) Uncertain PV power on a partly cloudy day

Figure 5.1: Realization of the uncertainties

BESS can be sized, i.e. the number of cells N the BESS consists of can be determined. A useful initial guess, ignoring internal resistance, battery inverter efficiency and cooling power is given by

$$N \approx \left\lceil \int_{t_0}^{t_f} \frac{\max\{0, P_{PV}(t) - P_{load}(t)\}}{P_{cell}^{nominal} \cdot \mathrm{DOD}} \, dt \right\rceil.$$

For the sake of sizing, we thus have to agree on a battery operation strategy, i.e. we have to agree on bounds $[SOC^{\min},\ SOC^{\max}]$ for the SOC. We recall that battery degradation is accelerated the higher the DOD is. For the SOC we choose to follow the standard

$$[SOC^{\min},\ SOC^{\max}] = [0.2,\ 0.8]. \tag{12}$$

The number of battery cells found to work well and used in this work is $N = 17\ 500$. We recall that higher temperatures also favor battery degradation. Hence, for battery thermal operation strategy, we choose not to follow the widely accepted recommendation [10] of $[T^{\min},\ T^{\max}] = [15\,^\circ\mathrm{C},\ 35\,^\circ\mathrm{C}]$. For mini-grid operation, choosing a narrower temperature range aligns well with optimizing performance and ensuring longevity since managing battery temperature within the desired range is achievable without excessive energy consumption. This is due to a mini-grid being a low C-rate application resulting in little Joule heat being generated compared to a high C-rate application. Hence, we choose

$$[T^{\min},\ T^{\max}] = [20\,^\circ\mathrm{C},\ 25\,^\circ\mathrm{C}]. \tag{13}$$

Finally, we impose $SOC_f = 0.5$ and $T_f = 22.5\,^\circ\mathrm{C}$. Throughout this section, the same uncertain demand P_{load} and the same uncertain ambient temperature T_{amb} is assumed; compare to Figure 5.1a and Figure 5.1b, respectively. For PV power, two scenarios are taken into consideration: a very sunny day, as shown in Figure 5.1c and a partly cloudy day, as illustrated in Figure 5.1d.

5.1 Results and discussion

The proposed energy management strategies illustrated in Figure 5.2 are each result of solving the discretized probabilistic OCP numerically w.r.t. increasing joint PLs $p = p_i \in \{0.5, 0.75, 0.95\}$ and cycling PLs $q = q_i = \min\{0.75, p_i\}$, $i = 1, 2$. The reader is referred to Table 2.1 and Table 2.2 for the thermodynamic parameters used for the numerical simulations.

The optimized control variables considering a sunny day are illustrated in Figures 5.4a, 5.4c, and 5.4e and the resulting state variables are depicted in Figure 5.5. Prescribed and actual (realized) PLs can be found in Table 5.1. Similarily, the optimized control variables for a partly cloudy day are depicted in Figures 5.4b, 5.4d and 5.4f. and the resulting state variables are depicted in Figure 5.6. Prescribed and actual (realized) PLs can be found in Table 5.2. A depiction of the power balance for sunny and partly cloudy day for the forecast can be seen in Figure 5.2a and Figure 5.2b, respectively.

On a sunny day, generally, the higher the desired reliability, the higher the usage of the DG and the higher the amount of excess power that has to be dumped as becomes very evident from Figure 5.4c and Figure 5.4e. In the early morning, when there is no PV power available, the DG has to be switched on in order to not violate the JCC on SOC by falling (in too many scenarios) below the lower bound on SOC. During mid-day, when there is PV power available, increasing the joint PL p_1 means that the amount of excess power P_{dump} to be dumped increases in order to not over-charge the battery (too frequently). The DG is switched on again in the evening due to the imposed CCC on SOC. The usage of DG in the evening increases even for non-increasing cycling PL q_1 as the joint PL p_1 is nonetheless rising: the excess power that has to be dumped in the (after-)noon is then missing in the evening again. Cooling takes place mostly during mid-day when there is PV power available and when it is hottest. At a first glance, there seems to be no clear ordering w.r.t. reliability level, c.f. Figure 5.4e. Taking a very close look reveals that the overall cooling power increases until the joint PL p_2 on battery temperature reaches a value of 0.75 and then starts to decrease. This is due to the cycling PL q_2 being kept constant after having reached a value of $q_2 = 0.75$. Simultaneously, the higher the joint PL p_2, the higher the cooling power in the early morning in order to not exceed the upper bound (too often). In the afternoon, cooling power is lower for higher joint PL p_2 in a maximal possible way without violating the JCC on the lower bound. For cooling in the evening, the DG has to run again. Thus, cooling is performed in the afternoon as much as possible such that the JCC on battery temperature is still met, i.e. the lower bound on battery temperature is not violated (too frequently).

Also on a partly cloudy day, generally, the higher the desired reliability, the higher the usage of DG, see Figure 5.4d. In contrast, there is no excess power at all for any PL, compare to Figure 5.4f. An important observation is that PLs on the JCC of SOC are not binding until very high probabilities. This is due to the CCC on SOC being the driving force: the higher the PL q_1 on the CCC, the more DG power has to be imported. Thus, the higher the cycling PL, the lower the realized probability for the JCC as the upper bound becomes active. This can be seen from Table 5.2. The CCC being the driving force is highlighted in Figure 5.3b, where the objective increases until PL $q_i = p_i = 0.75$, $i = 1, 2$ and afterwards nearly stays constant – as the cycling PL stays constant, too. Cooling is performed in a way that is just enough: the upper bound on battery temperature is the active one and cooling increases with increasing joint PL.

5.2 Conclusion and outlook

Given the task of finding an optimal energy management strategy for an isolated mini-grid, a probabilistic OCP taking into account has been set up and solved numerically using the concept of chance constraints.

As evident from Figure 5.3, the partly cloudy day comes at higher cost due to augmented need for DG power. DG usage on a partly cloudy day is driven by meeting the CCC on SOC. On a sunny day, compared to a partly cloudy day, there is an excess of power that needs to be dumped. Cooling on a sunny day is conducted such that cooling is minimal in the evening as for cooling in the evening the DG has to run. On a partly cloudy day cooling power is just enough to meet the JCC and CCC on battery temperature. The reader's attention is also

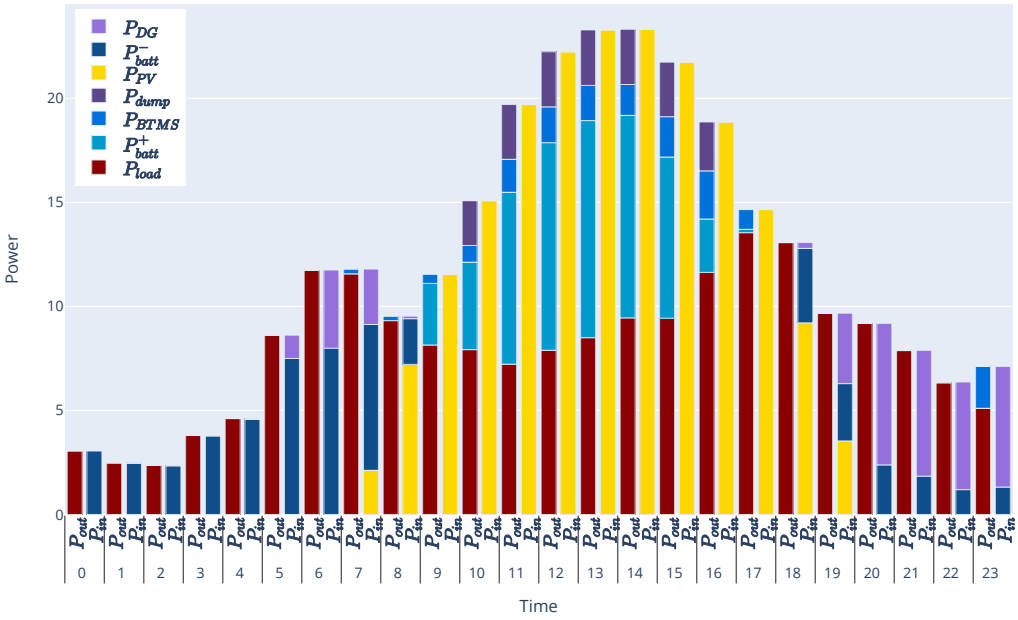

(a) On a sunny day

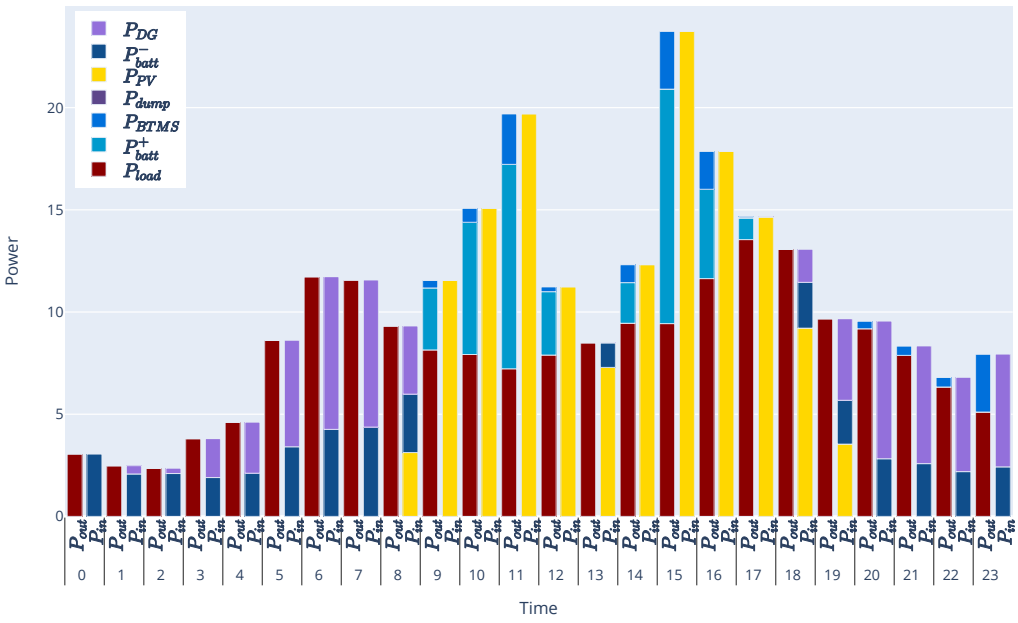

(b) On a partly cloudy day

Figure 5.2: Power balance for $p_1 = p_2 = 0.95$, $q_1 = q_2 = 0.75$ for the forecasts $\hat{P}_{PV}$, $\hat{P}_{load}$ and $\hat{T}_{amb}$.

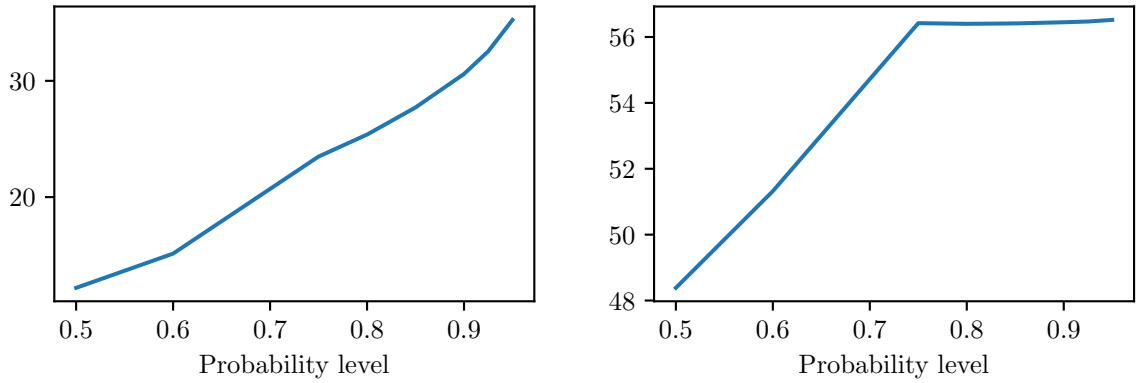

(a) On a sunny day

(b) On a partly cloudy day

Figure 5.3: Total DG power needed as a function of joint PL $p = p_1 = p_2$. The cycling PL $q = q_1 = q_2$ is given by $q = \min\{p, 0.75\}$.

drawn to the fact that usage of the DG is not necessarily unique as it could be shifted in time yielding pretty much the same results. This could be further addressed by refining fuel consumption of the DG. In addition, by introducing binary variables for switching on and off the DG, ramp-up rates of the DG can be included. A cold DG does not run as efficiently as a warm one [12].

The numerical results presented in the previous section indicate that the probabilistic OCP delivers an energy management strategy that strikes balance between reliability and cost. The higher the PL, the higher the operational costs and the operator may decide, based on these findings, which strategy and which reliability level to choose. The results indicate that the solution concept presented in this paper offers a generic good way of optimizing energy management. Nonetheless, the resulting energy management strategy heavily depends on the choice of parameters.

Having at hand those numerical results, there are a bunch of open questions. Most importantly, usage of the DG is pretty high. In addition to the fact that there is even an excess of power at some times, this indicates that the BESS is not sized very well. Also, deciding on battery (thermal) operation strategies can potentially be improved. This indicates that sizing and designing mini-grids and their operation can be further enhanced. This is ongoing work: set up and study a two-time scale optimization problem including battery degradation dynamics for the optimal design, i.e. layout and operation strategies, of stand-alone mini-grids.

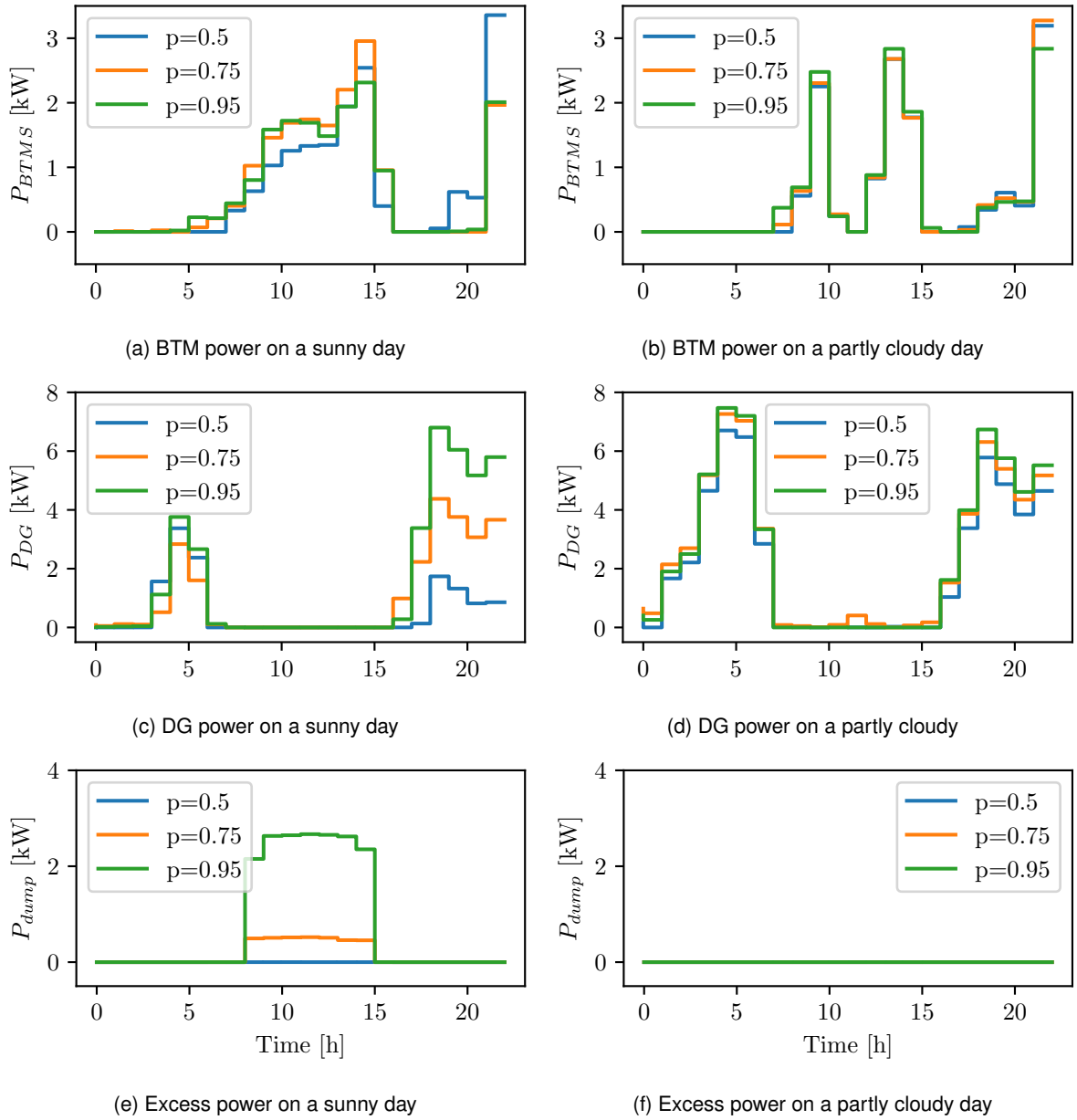

(a) BTM power on a sunny day

(b) BTM power on a partly cloudy day

(c) DG power on a sunny day

(d) DG power on a partly cloudy

(e) Excess power on a sunny day

(f) Excess power on a partly cloudy day

Figure 5.4: Optimized control variables for different joint probability levels p. The cycling probability levels are given by $q = \min\{0.75, p\}$.

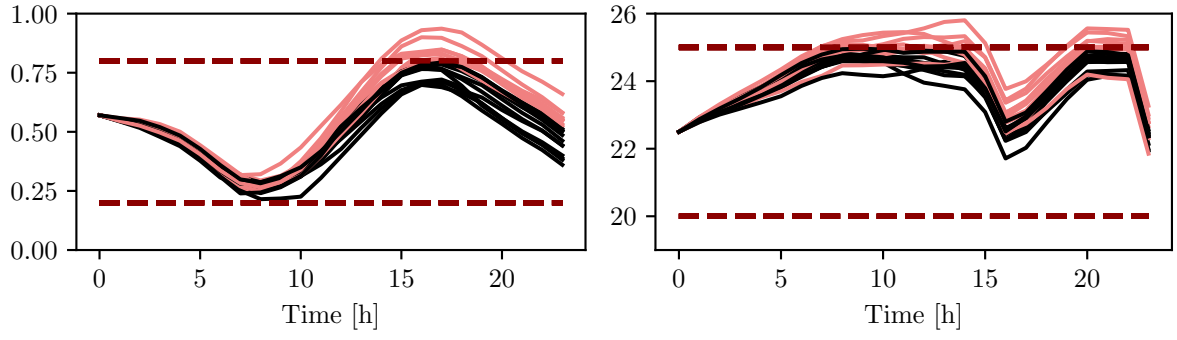

(a) SOC for $p_1 = 0.5$, $q_1 = 0.5$

(b) Battery temperature for $p_2 = 0.5$, $q_2 = 0.5$

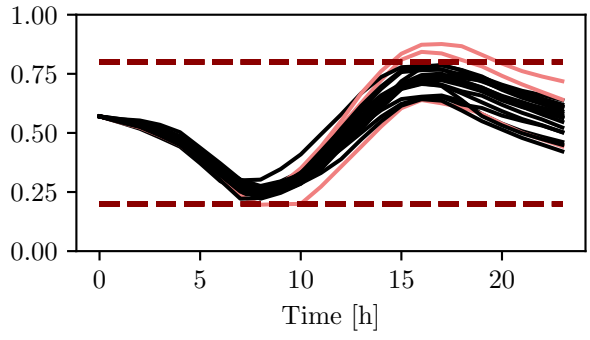

(c) SOC for $p_1 = 0.75$, $q_1 = 0.75$

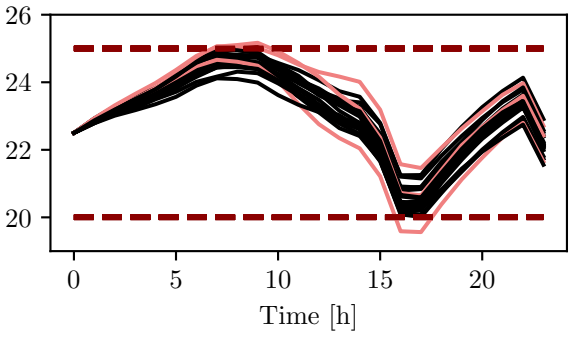

(d) Battery temperature for $p_2 = 0.75$, $q_2 = 0.75$

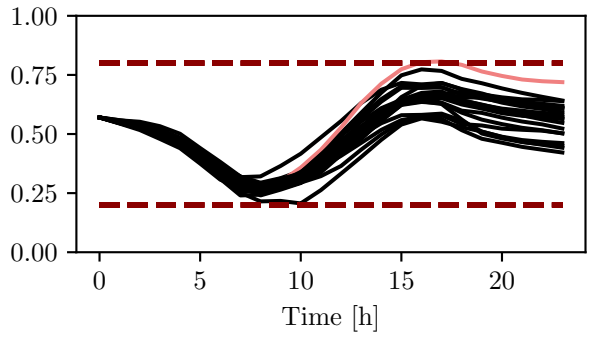

(e) SOC for $p_1 = 0.95$, $q_1 = 0.75$

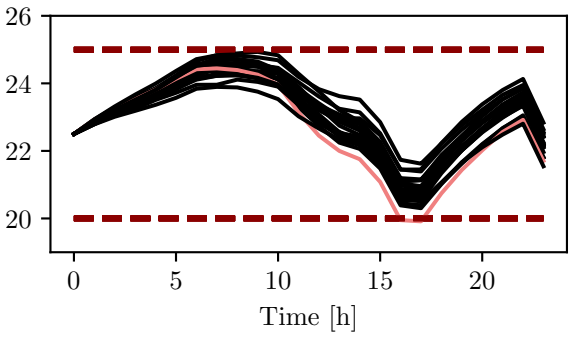

(f) Battery temperature for $p_2 = 0.95$, $q_2 = 0.75$

Figure 5.5: Resulting state variables on a sunny day. A total of 20 trajectories is plotted each. Black: trajectories that satisfy the joint chance constraint. Red: trajectories that do not satisfy the joint chance constraint.

Table 5.1: Prescribed and realized probability levels for SOC and battery cell temperature on a sunny day. Printed in bold: binding probability level.

$\mathbb{P}\big(SOC(t) \in [0.2, 0.8]\ \forall t\big)$	p_1	$\mathbb{P}\big(SOC(t_f) \geq 0.5\big)$	q_1
0.5	**0.5**	**0.5**	**0.5**
0.75	**0.75**	**0.75**	**0.75**
0.95	**0.95**	**0.75**	**0.75**
$\mathbb{P}\big(T_{cell}(t) \in [20, 25]\ \forall t\big)$	p_2	$\mathbb{P}\big(T_{cell}(t_f) \leq 22.5\big)$	q_2
0.5	**0.5**	**0.5**	**0.5**
0.75	**0.75**	**0.75**	**0.75**
0.95	**0.95**	**0.75**	**0.75**

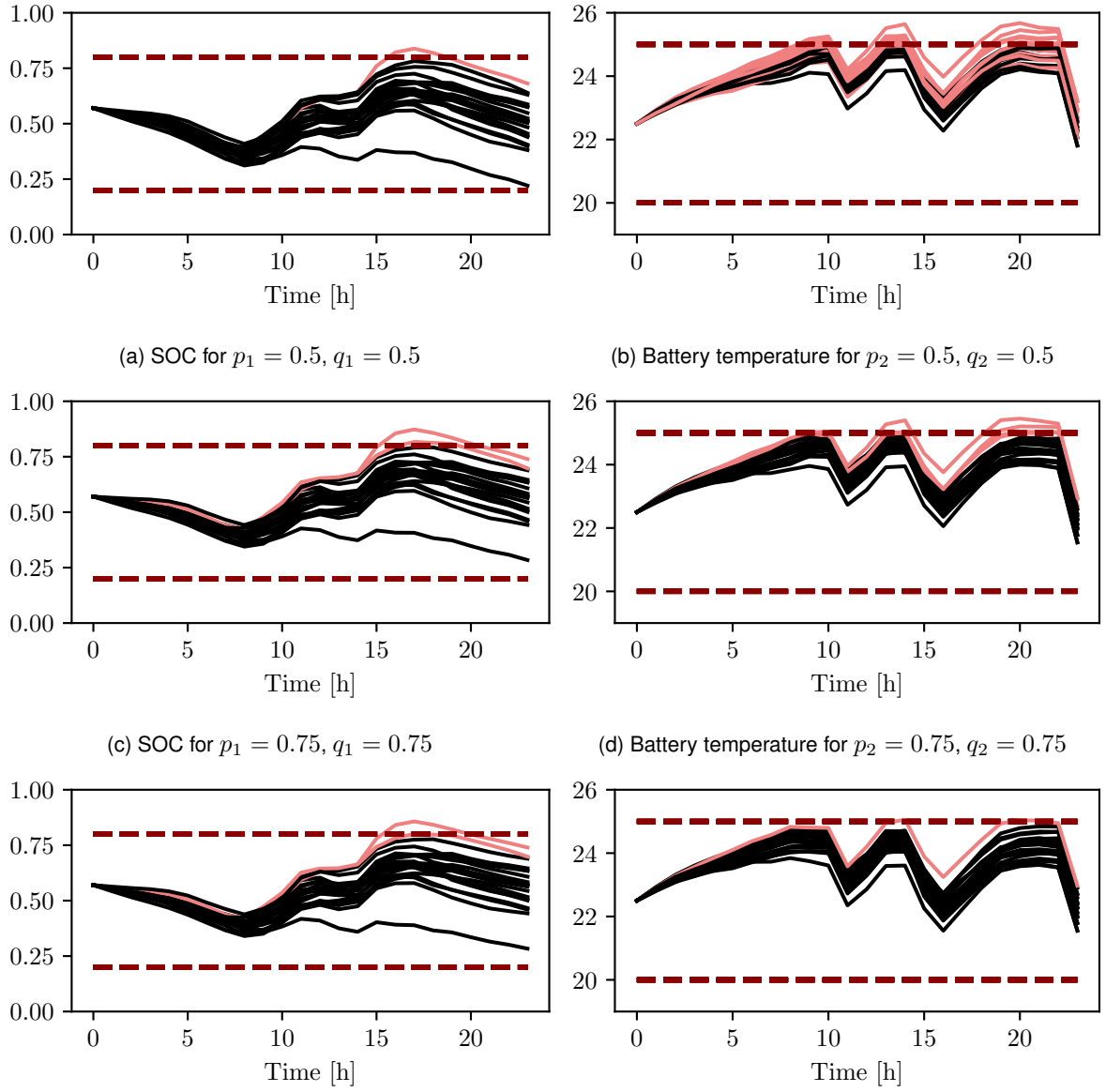

(a) SOC for $p_1 = 0.5$, $q_1 = 0.5$

(b) Battery temperature for $p_2 = 0.5$, $q_2 = 0.5$

(c) SOC for $p_1 = 0.75$, $q_1 = 0.75$

(d) Battery temperature for $p_2 = 0.75$, $q_2 = 0.75$

(e) SOC for $p_1 = 0.95$, $q_1 = 0.75$

(f) Battery temperature for $p_2 = 0.95$, $q_2 = 0.75$

Figure 5.6: State variables on a partly cloudy day. A total of 20 trajectories is plotted each. Black: trajectories that satisfy the joint chance constraint. Red: trajectories that do not satisfy the joint chance constraint.

Table 5.2: Prescribed and realized probability levels for battery cell temperature on a partly cloudy day. Printed in bold: binding probability levels.

$\mathbb{P}\big(SOC(t) \in [0.2, 0.8]\ \forall t\big)$	p_1	$\mathbb{P}\big(SOC(t_f) \geq 0.5\big)$	q_1
0.97	0.5	**0.5**	**0.5**
0.93	0.75	**0.75**	**0.75**
0.95	**0.95**	**0.75**	**0.75**
$\mathbb{P}\big(T_{cell}(t) \in [20, 25]\ \forall t\big)$	p_2	$\mathbb{P}\big(T_{cell}(t_f) \leq 22.5\big)$	q_2
0.5	**0.5**	**0.5**	**0.5**
0.75	**0.75**	**0.75**	**0.75**
0.95	**0.95**	**0.75**	**0.75**

Abbreviations

BESS	Battery energy storage system
BTMS	Battery thermal management system
CCC	Cycling chance constraint
DG	Diesel generator
DOD	Depth-of-discharge
ECM	Equivalent circuit model
JCC	Joint chance constraint
LIB	Lithium-ion battery
OCP	Optimal control problem
OCV	Open-circuit voltage
ODE	Ordinary differential equation
PL	Probability level
PV	Photovoltaic
RES	Renewable energy source
SOC	State-of-charge
SOH	State-of-health

Data availability

Data will be made available on reasonable request.

Software and tools used

The Python programming language was used to solve [22] the problem under consideration and to visualize the respective results.

References

[1] A. Charnes and W. W. Cooper. Chance-constrained programming. *Manag. Sci.*, 6(1):73–79, 1959.

[2] S. J. Drake, D. A. Wetz, J. K. Ostanek, S. P. Miller, J. M. Heinzel, and A. Jain. Measurement of anisotropic thermophysical properties of cylindrical li-ion cells. *J. Power Sources*, 252:298–304, 2014.

[3] M. Ecker, N. Nieto, S. Käbitz, J. Schmalstieg, H. Blanke, A. Warnecke, and D. W. Sauer. Calendar and cycle life study of Li(NiMnCo)O_2-based 18650 lithium-ion batteries. *J. Power Sources*, 248:839–851, 2014.

[4] J. Engels, B. Claessens, and G. Deconinck. Techno-economic analysis and optimal control of battery storage for frequency control services, applied to the german market. *Appl. Energy*, 242:1036–1049, 2019.

[5] C. Gotzes, H. Heitsch, R. Henrion, and R. Schultz. On the quantification of nomination feasibility in stationary gas networks with random load. *Math. Methods Oper. Res.*, 84:427–457, 2016.

[6] D. Halliday, R. Resnick, and J. Walker. *Fundamentals of Physics*. John Wiley & Sons Canada, Limited, New York, 2010.

[7] M. A. Hannan, A. Al-Shetwi, R. A. Begum, S. E. Young, M. M. Hoque, P. Ker, M. Mansur, and K. Alzaareer. The value of thermal management control strategies for battery energy storage in grid decarbonization: Issues and recommendations. *J. Clean. Prod.*, 276:124223, 2020.

[8] L. Lander, E. Kallitsis, A. Hales, J. S. Edge, A. Korre, and G. Offer. Cost and carbon footprint reduction of electric vehicle lithium-ion batteries through efficient thermal management. *Appl. Energy*, 289:116737, 2021.

[9] G. Liu, M. Starke, B. Xiao, X. Zhang, and K. Tomsovic. Microgrid optimal scheduling with chance-constrained islanding capability. *Electric Power Syst. Res.*, 145:197–206, 2017.

[10] S. Ma, M. Jiang, P. Tao, C. Song, J. Wu, J. Wang, T. Deng, and W. Shang. Temperature effect and thermal impact in lithium-ion batteries: A review. *Prog. Nat. Sci.: Mater. Int.*, 28(6):653–666, 2018.

[11] N. Ouanes, T. González Grandón, H. Heitsch, and R. Henrion. Optimizing the economic dispatch of weakly-connected mini-grids under uncertainty using joint chance constraints. Preprint no. 3069 (2023), Weierstrass Institute Berlin.

[12] R. Palma-Behnke, C. Benavides, F. Lanas, B. Severino, L. Reyes, J. Llanos, and D. Sáez. A microgrid energy management system based on the rolling horizon strategy. *IEEE Trans. Smart Grid*, 4(2):996–1006, 2013.

[13] G. Plett. *Battery management systems, Volume I: Battery modeling*. Power engineering/power electronics. Artech House, Norwood, MA, 2015.

[14] A. Prékopa. *Stochastic programming*. Mathematics and its applications ; v. 324. Kluwer Academic Publishers, Dordrecht, 1995.

[15] M. A. Vaziri Rad, A. Kasaeian, X. Niu, K. Zhang, and O. Mahian. Excess electricity problem in off-grid hybrid renewable energy systems: A comprehensive review from challenges to prevalent solutions. *Renew. Energy*, 212:538–560, 2023.

[16] H. Rahimi-Eichi, U. Ojha, F. Baronti, and M. Chow. Battery management system: An overview of its application in the smart grid and electric vehicles. *IEEE Ind. Electron. Mag.*, 7(2):4–16, 2013.

[17] D. M. Rosewater, D. A. Copp, T. A. Nguyen, R. H. Byrne, and S. Santoso. Battery energy storage models for optimal control. *IEEE Access*, 7:178357–178391, 2019.

[18] J. Schmalstieg, S. Käbitz, M. Ecker, and D. U. Sauer. A holistic aging model for Li(NiMnCo)O_2 based 18650 lithium-ion batteries. *J. Power Sources*, 257:325–334, 2014.

[19] R. H. Shumway and D. S. Stoffer. *Time Series Analysis and Its Applications*. Springer Texts in Statistics. Springer, Cham, 2000.

[20] W. van Ackooij and R. Henrion. Gradient formulae for nonlinear probabilistic constraints with gaussian and gaussian-like distributions. *SIAM J. Optim.*, 24(4):1864–1889, 2014.

[21] W. van Ackooij and R. Henrion. (sub-)gradient formulae for probability functions of random inequality systems under gaussian distribution. *J. Uncertain. Quantif.*, 5:63–87, 2017.

[22] Pauli Virtanen, Ralf Gommers, Travis E. Oliphant, Matt Haberland, Tyler Reddy, David Cournapeau, Evgeni Burovski, Pearu Peterson, Warren Weckesser, Jonathan Bright, Stéfan J. van der Walt, Matthew Brett, Joshua Wilson, K. Jarrod Millman, Nikolay Mayorov, Andrew R. J. Nelson, Eric Jones, Robert Kern, Eric Larson, C J Carey, İlhan Polat, Yu Feng, Eric W. Moore, Jake VanderPlas, Denis Laxalde, Josef Perktold, Robert Cimrman, Ian Henriksen, E. A. Quintero, Charles R. Harris, Anne M. Archibald, Antônio H. Ribeiro, Fabian Pedregosa, Paul van Mulbregt, and SciPy 1.0 Contributors. SciPy 1.0: Fundamental Algorithms for Scientific Computing in Python. *Nat. Methods*, 17:261–272, 2020.

[23] B. Zhao, Y. Shi, , X. Dong, W. Luan, and J. Bornemann. Short-term operation scheduling in renewable-powered microgrids: A duality-based approach. *IEEE Trans. Sustain. Energy*, 5(1):209–217, 2014.